J|A|C|S ARTICLES

Published on Web 05/25/2010

Sensitive Efficiency of Photoinduced Electron Transfer to Band Gaps of Semiconductive Single-Walled Carbon Nanotubes with Supramolecularly Attached Zinc Porphyrin Bearing Pyrene Glues

Eranda Maligaspe,[†] Atula S. D. Sandanayaka,[‡] Taku Hasobe,*[,⊥,||] Osamu Ito,*[,§] and Francis D'Souza*[,†]

Department of Chemistry, Wichita State University, 1845 Fairmount, Wichita, Kansas 67260-0051, School of Materials Science, Japan Advanced Institute of Science and Technology (JAIST), Nomi, Ishikawa 923-1292, Japan, Department of Chemistry, Faculty of Science and Technology, Keio University, Yokohama 223-8522, Japan, PRESTO, JST, 4-1-8, Kawaguchi, Saitama 332-0012, Japan, and Institute of Multidisciplinary Research for Advanced Materials, Tohoku University, Katahira, Sendai 980-8577 Japan

Received March 2, 2010; E-mail: hasobe@chem.keio.ac.jp; francis.dsouza@wichita.edu

Abstract: Photoinduced electron transfer in self-assembled single-walled carbon nanotube (SWNT)/zinc porphyrin (ZnP) hybrids utilizing (7,6)- and (6,5)-enriched SWNTs has been investigated. Toward this, first, zinc porphyrin was covalently functionalized to possess four pyrene entities (ZnP(pyr)$_4$). Exfoliation of the semiconducting nanotube bundles occurred due to $\pi-\pi$-type interactions with the pyrene and porphyrin entities in organic solvents. The nanohybrids thus formed were isolated and characterized by TEM, UV−visible−near-IR, and Raman spectroscopy. Free-energy calculations suggested the possibility of electron transfer in both the (7,6)- and (6,5)-possessing ZnP(pyr)$_4$/SWNT nanohybrids. Accordingly, fluorescence studies revealed efficient quenching of the singlet excited state of ZnP in the nanohybrids, originating from the charge separation, as confirmed by observation of a ZnP π-cation radical in transient absorption spectra. The rates of charge separation were found to be slightly higher for (7,6)-SWNT-derived hybrids compared to the (6,5)-SWNT-derived hybrids. Charge recombination revealed an opposite effect, indicating that the (7,6)-SWNTs are slightly better for charge stabilization compared to the (6,5)-SWNTs. The present nanohybrids were further utilized to photochemically reduce the hexyl viologen dication in the presence of a sacrificial electron donor in an electron-pooling experiment, offering additional proof for the occurrence of photoinduced charge separation and potential utilization of these materials in light-energy-harvesting applications. Finally, solar cells constructed using the ZnP/SWNT hybrids revealed higher efficiency for the ZnP(pyr)$_4$/(7,6)-SWNT hybrid with narrower nanotube band gap compared with the ZnP(pyr)$_4$/(6,5)-SWNT having a relatively wider band gap.

Introduction

In recent years, major research effort has been devoted to understanding the physicochemical properties of carbon nanotubes, a new allotropic form of carbon,[1] with the intention of developing nanomaterial-based devices that could outline future technologies.[2−4] In this context, single-walled carbon nanotubes (SWNTs) have emerged as attractive candidates because of their outstanding physical, chemical, and mechanical properties.[2] The SWNTs consist of graphitic layers wrapped seamlessly into cylinders that originate from defined sections of two-dimensional graphene sheets. The structure of SWNTs relates to a pair of indices (n,m), referring to their diameter and chirality.[5] SWNTs are semiconducting, except for those in which the difference between n and m is a multiple of 3, and those are metallic. Recent efforts involving noncovalent chemical functionalization

[†] Wichita State University.
[‡] JAIST.
[⊥] Keio University.
[||] PRESTO, JST.
[§] Tohoku University.

(1) (a) Iijima, S. *Nature* **1991**, *354*, 56. (b) Iijima, S.; Ichihashi, T. *Nature* **1993**, *364*, 737.
(2) (a) Harris, P. J. F. *Carbon Nanotubes and Related Structures: New Materials for the Twenty-First Century*; Cambridge University Press: Cambridge, UK, 2001. (b) *Carbon Nanotubes: Synthesis, Structure and Applications*; Dresselhaus, M. S., Dresselhaus, G., Avouris, Ph., Eds.; Springer Publishing: New York, 2001. (c) Special issue on Carbon Nanotubes. *Acc. Chem. Res.* **2002**, *35*, 997.
(3) (a) Reich, S.; Thomsen, C.; Maultzsch, J. *Carbon Nanotubes: Basic Concepts and Physical Properties*; Wiley-VCH: Weinheim, 2004; (b) Roth, S.; Carroll, D. *One-Dimensional Metals: Conjugated Polymers, Organic Crystals, Carbon Nanotubes*; Wiley-VCH: Weinheim, Germany, 2004. (c) Meyyappan, M. *Carbon Nanotubes, Science and Application*; Wiley-VCH: Weinheim, Germany, 2006.
(4) (a) *Introduction to Nanotechnology*; Poole, C. P., Owens, F. J., Eds.; Wiley-Interscience: Weinheim, 2003. (b) *Nanophysics and Nanotechnology: An Introduction to Modern Concepts in Nanoscience*; Wolf, E. L., Ed.; John Wiley & Sons: New York, 2004.
(5) (a) Mamada, N.; Sawada, S.; Oshiyama, A. *Phys. Rev. Lett.* **1992**, *68*, 1579. (b) Saito, R.; Dresselhaus, G.; Dresselhaus, M. S. *Physical Properties of Carbon Nanotubes*; Imperial College Press: London, 1998.

 10.1021/ja101776p © 2010 American Chemical Society

and physical techniques have resulted in the separation of metallic and semiconducting SWNTs according their (*n*,*m*) index.[6−9]

Among the different applications of SWNTs, the unique structure and the presence of extended π-delocalization have made them attractive candidates to develop light-energy-harvesting and photovoltaic materials.[10] Consequently, incorporation of SWNTs into donor−acceptor ensembles for the study of light-induced electron transfer has become an active area of research. Accordingly, various elegant covalently linked and non-covalently assembled donor−acceptor hybrids containing SWNT have been reported.[10−20] However, all of these studies used mixture of SWNTs that were both metallic and semiconducting, with different (*n*,*m*) indices, making it impossible to derive meaningful and conclusive structure−reactivity relationships.

In the present study, we have overcome this barrier by constructing donor−acceptor hybrids made from semiconducting SWNTs of largely a single (*n*,*m*) index type; that is, two types of semiconducting nanotubes, viz., (6,5) and (7,6), having different band gaps (difference up to 0.1 eV) have been utilized. Additionally, non-covalent self-assembly involving $\pi-\pi$ interactions between the donor−acceptor entities has been employed since this method would not destroy the electronic structure of nanotubes significantly.[21] To accomplish this, the donor, zinc porphyrin, has been functionalized with four pendant pyrene entities (Figure 1; ZnP(pyr)$_4$). Due to the presence of four interacting pyrene entities on the nanotubes' surface, stable ZnP(pyr)$_4$/SWNT hybrids are expected to form. As demonstrated here, this is indeed the case; additionally, the newly formed ZnP(pyr)$_4$/SWNT hybrids have allowed us to investigate the

(6) (a) O'Connell, M. J.; Bachilo, S. M.; Huffman, C. B.; Moore, V. C.; Strano, M. S.; Haroz, E. H.; Rialon, K. L.; Boul, P. J.; Noon, W. H.; Kittrell, C.; Ma, J. P.; Hauge, R. H.; Weisman, R. B.; Smalley, R. E. *Science* **2002**, *297*, 593. (b) Zheng, M.; Jagota, A.; Strano, M. S.; Santos, A. P.; Barone, P.; Chou, S. G.; Diner, B. A.; Dresselhaus, M. S.; McLean, R. S.; Onoa, G. B.; Samsonidze, G. G.; Semke, E. D.; Usrey, M.; Walls, D. J. *Science* **2003**, *302*, 1545. (c) Strano, M. S.; Dyke, C. A.; Usrey, M. L.; Barone, P. W.; Allen, M. J.; Shan, H. W.; Kittrell, C.; Hauge, R. H.; Tour, J. M.; Smalley, R. E. *Science* **2003**, *301*, 151.

(7) (a) Bachilo, S. M.; Balzano, L.; Herrera, J. E.; Pompeo, F.; Resasco, D. E.; Weisman, R. B. *J. Am. Chem. Soc.* **2003**, *125*, 11186. (b) Chattopadhyay, D.; Galeska, L.; Papadimitrakopoulos, F. *J. Am. Chem. Soc.* **2003**, *125*, 3370. (c) Arnold, M. S.; Stupp, S. I.; Hersam, M. C. *Nano Lett.* **2005**, *5*, 713. (d) An, K. H.; Park, J. S.; Yang, C. M.; Jeong, S. Y.; Lim, S. C.; Kang, C.; Son, J. H.; Jeong, M. S.; Lee, Y. H. *J. Am. Chem. Soc.* **2005**, *127*, 5196. (e) Maeda, Y.; et al. *J. Am. Chem. Soc.* **2005**, *127*, 10287–10290.

(8) (a) Menard-Moyon, C.; Izard, N.; Doris, E.; Mioskowski, C. *J. Am. Chem. Soc.* **2006**, *128*, 6552. (b) Arnold, M. S.; Green, A. A.; Hulvat, J. F.; Stupp, S. I.; Hersam, M. C. *Nat. Nanotechnol.* **2006**, *1*, 60. (c) Hersam, M. C. *Nat. Nanotechnol.* **2008**, *3*, 387. (d) Hwang, J. Y.; Nish, A.; Doig, J.; Douven, S.; Chen, C. W.; Chen, L. C.; Nicholas, R. J. *J. Am. Chem. Soc.* **2008**, *130*, 3543.

(9) (a) Collins, P. C.; Arnold, M. S.; Avouris, P. *Science* **2001**, *292*, 706. (b) Krupke, R.; Hennrich, F.; von Lohneysen, H.; Kappes, M. M. *Science* **2003**, *301*, 344. (c) Zhang, G. Y.; Qi, P. F.; Wang, X. R.; Lu, Y. R.; Li, X. L.; Tu, R.; Bangsaruntip, S.; Mann, D.; Zhang, L.; Dai, H. J. *Science* **2006**, *314*, 974. (d) Song, J. W.; Seo, H. W.; Park, J. K.; Kim, J. E.; Cho, D. G.; Han, C. S. *Curr. Appl. Phys.* **2008**, *8*, 725. (e) Qui, H.; Maeda, Y.; Akasaka, T. *J. Am. Chem. Soc.* **2009**, *131*, 16529.

(10) (a) Sgobba, V.; Rahman, G. M. A.; Guldi, D. M. In *Carbon Nanotubes in Electron Donor-Acceptor Nanocomposites, Chemistry of Carbon Nanotubes*; Basiuk, V. A., Ed.; American Scientific Publishers: Stevenson Ranch, CA, 2006. (b) Sgobba, V.; Rahman, G. M. A.; Ehli, C.; Guldi, D. M. Covalent and Non-covalent Approaches Toward Multifunctional Carbon Nanotubes Materials In *Fullerenes-Principles and Applications*; Langa, F., Nierengarten, J. F., Eds.; Royal Society of Chemistry: Cambridge, UK, 2007. (c) Chitta, R.; D'Souza, F. *J. Mater. Chem.* **2008**, *18*, 1440. (d) Sgobba, V.; Guldi, D. M. *Chem. Soc. Rev.* **2009**, *38*, 165.

(11) (a) Kataura, H.; Maniwa, Y.; Suzuki, S.; Achiba, Y. *Jpn. J. Appl. Phys.* **2001**, *40*, L1229. (b) Georgakilas, V.; Kordatos, K.; Prato, M.; Guldi, D. M.; Holzinger, M.; Hirsch, A. *J. Am. Chem. Soc.* **2002**, *124*, 760. (c) Cao, L.; Chen, H.; Wang, M.; Sun, J.; Zhang, X.; Kong, F. *J. Phys. Chem. B* **2002**, *106*, 8971. (d) Star, A.; Steuerman, D. W.; Heath, J. R.; Stoddart, J. F. *Angew. Chem., Int. Ed.* **2002**, *41*, 2508. (e) Dyke, C. A.; Tour, J. M. *J. Am. Chem. Soc.* **2003**, *125*, 1156. (f) Freitag, M.; Martin, Y.; Misewich, J. A.; Martel, R.; Avouris, P. *Nano Lett.* **2003**, *3*, 1067.

(12) (a) Holzinger, M.; Abraham, J.; Whelan, P.; Graupner, R.; Ley, L.; Hennrich, F.; Kappes, M.; Hirsch, A. *J. Am. Chem. Soc.* **2003**, *125*, 8566. (b) Murakami, H.; Nomura, T.; Nakashima, N. *Chem. Phys. Lett.* **2003**, *378*, 481. (c) Guldi, D. M.; Marcaccio, M.; Paolucci, D.; Paolucci, F.; Tagmatarchis, N.; Tasis, D.; Vazquez, E.; Prato, M. *Angew. Chem., Int. Ed.* **2003**, *42*, 4206. (d) Fukushima, T.; Kosaka, A.; Ishimura, Y.; Yamamoto, T.; Takigawa, T.; Ishii, N.; Aida, T. *Science* **2003**, *300*, 2072. (e) Sun, J.; Gao, L.; Iwasa, M. *Chem. Commun.* **2004**, 832.

(13) (a) Robel, I.; Bunker, B. A.; Kamat, P. V. *Adv. Mater.* **2004**, *17*, 2458. (b) Campidelli, S.; Sooambar, C.; Lozano, Diz, E.; Ehli, C.; Guldi, D. M.; Prato, M. *J. Am. Chem. Soc.* **2006**, *128*, 12544. (c) Herranz, M. A.; Martin, N.; Campidelli, S.; Prato, M.; Brehm, G.; Guldi, D. M. *Angew. Chem., Int. Ed.* **2006**, *45*, 4478. (d) Zheng, M.; Rostovtsev, V. V. *J. Am. Chem. Soc.* **2006**, *128*, 7702.

(14) (a) D'Souza, F.; Chitta, R.; Sandanayaka, A. S. D.; Subbaiyan, N. K.; D'Souza, L.; Araki, Y.; Ito, O. *J. Am. Chem. Soc.* **2007**, *129*, 15865. (b) Hasobe, T.; Maruta, H.; Kamat, P. V. *J. Phys. Chem. C* **2007**, *111*, 16626. (c) Chitta, R.; Sandanayaka, A. S. D.; Schumacher, A. L.; D'Souza, L.; Araki, Y.; Ito, O.; D'Souza, F. *J. Phys. Chem. C* **2007**, *111*, 6947. (d) Ballesteros, B.; De la Torre, G.; Ehli, C.; Rahman, G. M.; Aminur, A.-R. F.; Guldi, D. M.; Torres, T. *J. Am. Chem. Soc.* **2007**, *129*, 5061. (e) D'Souza, F.; Chitta, R.; Sandanayaka, A. S. D.; Subbaiyan, N. K.; D'Souza, L.; Araki, Y.; Ito, O. *Chem.−Eur. J.* **2007**, *13*, 8277. (f) Long, D.; Wu, G.; Wu, A. *J. Phys. Chem. C* **2008**, *112*, 13000. (g) Hu, L.; Zhao, Y. L.; Ryu, K.; Zhou, C.; Stoddart, J. F.; Gruner, G. *Adv. Mater.* **2008**, *20*, 939.

(15) (a) Li, H.; Zhou, B.; Lin, Y.; Gu, L.; Wang, W.; Fernando, K. A. S.; Kumar, S.; Allard, L. F.; Sun, Y.-P. *J. Am. Chem. Soc.* **2004**, *126*, 1014. (b) Guldi, D. M.; Taieb, H.; Rahman, G. M. A.; Tagmatarchis, N.; Prato, M. *Adv. Mater.* **2005**, *17*, 871. (c) Satake, A.; Miyajima, Y.; Kobuke, Y. *Chem. Mater.* **2005**, *17*, 716. (d) Robel, I.; Bunker, B. A.; Kamat, P. V. *Adv. Mater.* **2005**, *17*, 2458. (e) Chen, J.; Collier, C. P. *J. Phys. Chem. B* **2005**, *109*, 7605.

(16) (a) Hasobe, T.; Fukuzumi, S.; Kamat, P. V. *J. Phys. Chem. B* **2006**, *110*, 25477. (b) Hasobe, T.; Fukuzumi, S.; Kamat, P. V. *Angew. Chem., Int. Ed.* **2006**, *45*, 755. (c) Hasobe, T. *Phys. Chem. Chem. Phys.* **2010**, *12*, 44.

(17) (a) Guldi, D. M.; Rahman, G. M. A.; Ramey, J.; Marcaccio, M.; Paolucci, D.; Paolucci, F.; Qin, S.; Ford, W. T.; Balbinot, D.; Jux, N.; Tagmatarchis, N.; Prato, M. *Chem. Commun.* **2004**, 2034. (b) Li, H.; Martin, R. B.; Harruff, B. A.; Carino, R. A.; Sun, Y.-P. *Adv. Mater.* **2004**, *16*, 896. (c) Guldi, D. M.; Rahman, G. M. A.; Jux, N.; Tagmatarchis, N.; Prato, M. *Angew. Chem., Int. Ed.* **2004**, *43*, 5526. (d) Guldi, D. M.; Rahman, G. M. A.; Prato, M.; Jux, N.; Qin, S.; Ford, W. T. *Angew. Chem., Int. Ed.* **2005**, *44*, 2015.

(18) (a) Baskaran, D.; Mays, J. W.; Zhang, X. P.; Bratcher, M. S. *J. Am. Chem. Soc.* **2005**, *127*, 6916. (b) Guo, Z.; Du, F.; Ren, D.; Chen, Y.; Zheng, J.; Liu, Z.; Tian, J. *J. Mater. Chem.* **2006**, *16*, 3021. (c) Alvaro, M.; Atienzar, P.; de la Cruz, P.; Delgado, J. L.; Troiani, V.; Garcia, H.; Langa, F.; Palkar, A.; Echegoyen, L. *J. Am. Chem. Soc.* **2006**, *128*, 6626.

(19) (a) Guldi, D. M.; Rahman, G. M. A.; Qin, S.; Tchoul, M.; Ford, W. T.; Marcaddio, M.; Paolucci, D.; Paolucci, F.; Campidelli, S.; Prato, M. *Chem.−Eur. J.* **2006**, *12*, 2152. (b) Guldi, D. M.; Menna, E.; Maggini, M.; Marcaccio, M.; Paolucci, D.; Paolucci, F.; Campidelli, S.; Prato, M.; Rahman, G. M.; Shergna, S. *Chem.−Eur. J.* **2006**, *12*, 3975. (c) Herranz, A.; Martin, N.; Campidelli, S.; Prato, M.; Brehm, G.; Guldi, D. M. *Angew. Chem., Int. Ed.* **2006**, *45*, 4478.

(20) (a) Qin, S.; Qin, D.; Ford, W. T.; Herrera, J. E.; Resasco, D. E.; Bachilo, S. M.; Weisman, R. B. *Macromolecules* **2004**, *35*, 3965. (b) Guldi, D. M.; Rahman, G. M. A.; Sgobba, V.; Kotov, N. A.; Bonifazi, D.; Prato, M. *J. Am. Chem. Soc.* **2006**, *128*, 2315. (c) Rahman, G. M. A.; Troeger, A.; Sgobba, V.; Guldi, D. M.; Jux, N.; Tchoul, M. N.; Ford, W. T.; Mateo-Alonso, A.; Prato, M. *Chem.−Eur. J.* **2008**, *14*, 8837. (d) Sandanayaka, A. S. D.; Chitta, R.; Subbaiyan, N. K.; D'Souza, L.; Ito, O.; D'Souza, F. *J. Phys. Chem. C* **2009**, *113*, 13425.

(21) (a) Chen, R. J.; Zhang, Y.; Wang, D.; Dai, H. *J. Am. Chem. Soc.* **2001**, *123*, 3838. (b) Simmons, T. J.; Bult, J.; Hashim, D. P.; Linhardt, R. J.; Ajayan, P. M. *ACS Nano* **2009**, *3*, 865.

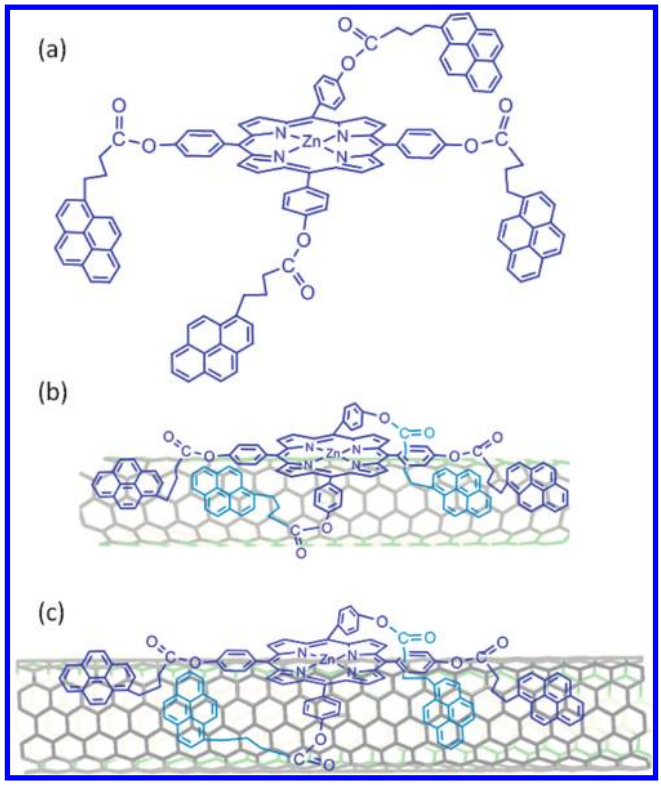

Figure 1. (a) Structure of the pyrene-appended zinc porphyrin donor. (b) ZnP(pyr)$_4$/(6,5)-SWNT and (c) ZnP(pyr)$_4$/(7,6)-SWNT donor−acceptor hybrids obtained as a result of $\pi-\pi$ interactions of the entities.

photoinduced electron transfer and to compare the electron acceptor behavior of the two types of nanotubes employed. Finally, photoelectrochemical responses of these ZnP(pyr)$_4$/SWNT nanohybrids have been tested.

Results and Discussion

The ZnP(pyr)$_4$/(6,5)-SWNT and ZnP(pyr)$_4$/(7,6)-SWNT hybrids were prepared by treating zinc porphyrin appended with pyrene entities, ZnP(pyr)$_4$, with SWNTs (see Experimental Section for details). Figure 2 shows transmission electron microscopy (TEM) images of the ZnP(pyr)$_4$-bound (6,5)- and (7,6)-SWNTs. The SWNT bundles were found to be loosened upon treatment with ZnP(pyr)$_4$, although intertwining during TEM sample preparation was observed. This suggests an appreciable decrease in SWNT stacking as compared with that in the untreated pristine SWNT samples. Each SWNT appeared thickened with a blur, probably by the adsorbed molecules. To a large extent, ZnP(pyr)$_4$/(6,5)-SWNT and ZnP(pyr)$_4$/(7,6)-SWNT hybrids were found to be free from impurities.

The samples were also characterized using laser Raman spectroscopy to obtain spectroscopic insight into the electronic structure of the SWNT in the ZnP(pyr)$_4$/(6,5)-SWNT and ZnP(pyr)$_4$/(7,6)-SWNT nanohybrids. In the Raman spectra of (6,5)-SWNT and (7,6)-SWNT, the characteristic radial breathing mode (RBM) bands in the 100−400 cm^{-1} region, disorder-induced D-mode in the 1350 cm^{-1} region, and Raman-allowed tangential G-bands in the 1500−1600 cm^{-1} region were expected.[22] As shown in Figure 3, the pristine (6,5)- and (7,6)-SWNTs revealed all of these Raman bands, and their values agreed well with the literature reports.[23] Interestingly, the Raman spectra of the noncovalently functionalized ZnP(pyr)$_4$/(6,5)-SWNT and ZnP(pyr)$_4$/(7,6)-SWNT revealed no significant shift on the peak position, only changing the relative intensities (300 vs 1570 cm^{-1} for (6,5)-SWNT and 170 vs 1570 cm^{-1} for (7,6)-SWNT). This implies that the electronic structures of the (6,5)-SWNT and (7,6)-SWNT are intact after being noncovalently functionalized with ZnP(pyr)$_4$.

Optical Absorption and Emission Studies. Figure 4 shows the optical absorption spectra of ZnP(pyr)$_4$/(6,5)-SWNT and ZnP(pyr)$_4$/(7,6)-SWNT in the UV−vis region in dimethylformamide (DMF). Absorption bands of the semiconducting (6,5)-SWNTs in the hybrids are at 583 and 1022 nm, and those of the (7,6)-SWNTs are at 667 and 1170 nm, respectively, showing red-shifts by 400−600 cm^{-1} from the pristine peaks,[24] due to their interaction with a π-electron of ZnP(pyr)$_4$. From the longest absorption edges, the band gap can be evaluated to be 1.21 and 1.05 eV, respectively, which also showed narrowing of 0.06−0.08 eV, due to the interaction with a π-electron of ZnP(pyr)$_4$. The ZnP(pyr)$_4$/(6,5)-SWNT and ZnP(pyr)$_4$/(7,6)-SWNT hybrids also showed Soret and Q bands of ZnP in the 420 and 550 nm regions, with UV bands corresponding to the pyrene moieties.[9e] As for the Soret band of the ZnP units at 420 nm, peak position shows appreciable shift, and spectral broadenings, suggesting weak interaction with SWNT.

Several studies have attempted to estimate the redox potentials (E_{ox} and E_{red}) of nanotubes using techniques such as scanning tunneling spectroscopy, redox titrimetry, photoluminescence, and spectroelectrochemistry.[25−27] Nakashima and co-workers[27] reported redox potentials of 15 isolated individual SWNTs having their own chirality indices based on Nernst analysis of the *in situ* spectroelectrochemical data. The work function of the SWNTs obtained experimentally agreed well with those calculated on the basis of first-principles.[27] The reported E_{ox} and E_{red} for the (6,5)-SWNT were 5.08 and 4.01 V vs vacuum, corresponding to a HOMO−LUMO gap of 1.07 eV. The E_{ox} and E_{red} for the (7,6)-SWNT were 4.94 and 4.03 V vs vacuum, with a HOMO−LUMO gap of 0.91 eV. The wider band gaps for (6,5)-SWNT than for (7,6)-SWNT estimated from the absorption bands is supported by these reported HOMO−LUMO gaps.

(22) Dresselhaus, M. S.; Dresselhaus, G.; Jorio, A.; Souza Filho, A. G.; Saito, R. *Carbon* **2002**, *40*, 2043.

(23) (a) Herrera, J. E.; Resasco, D. E. *Chem. Phys. Lett.* **2003**, *376*, 302. (b) Herrera, J. E.; Pompeo, B. F.; Resasco, D. E. *J. Nanosci. Nanotechnol.* **2003**, *3*, 1. (c) Jorio, A.; Santos, A. P.; Ribeiro, H. B.; Fantini, C.; Souza, M.; Vieira, J. P. M.; Furtado, C. A.; Jiang, J.; Saito, R.; Balzano, L.; Resasco, D. E.; Pimenta, M. A. *Phys. Rev. B* **2005**, *72*, 075207. (d) Hennrich, F.; Krupke, R.; Lebedkin, S.; Arnold, K.; Fischer, R.; Resasco, D. E.; Kappes, M. M. *J. Phys. Chem. B* **2005**, *109*, 10567.

(24) (a) Weisman, R. B.; Bachilo, S. M. *Nano Lett.* **2003**, *3*, 1234. (b) Luo, Z.; Pfefferle, L. D.; Haller, G. L.; Papadimitrakopoulos, F. *J. Am. Chem. Soc.* **2006**, *128*, 15511.

(25) (a) Okazaki, K.-I.; Nakato, Y.; Murakoshi, K. *Phys. Rev. B* **2003**, *68*, 35434. (b) Wilder, J. W. G.; Venema, L. C.; Rinzier, A. G.; Smalley, R. E.; Dekker, C. *Nature* **1998**, *391*, 59. (c) O'Connell, M. J.; Eibergen, E. E.; Doorn, S. K. *Nat. Mater.* **2005**, *4*, 412. (d) McDonald, T. J.; Svedruzic, D.; Kim, Y.-H.; Blackburn, J. L.; Zhang, S. B.; King, P. W.; Heben, M. J. *Nano Lett.* **2008**, *8*, 1783.

(26) (a) Kavan, L.; Dunsch, L. Electrochemistry of Carbon Nanotubes. In *Carbon Nanotubes: Advanced Topics in the Synthesis Structure, Properties and Applications*, Vol. 111; Springer: Berlin, 2008. (b) Paolucci, D.; Franco, M. M.; Iurlo, M.; Marcaccio, M.; Prato, M.; Zerbetto, F.; Penicaud, A.; Paolucci, F. *J. Am. Chem. Soc.* **2008**, *130*, 7393. (c) Ehli, C.; Oelsner, C.; Guldi, D. M.; Mateo-Alonso, A.; Prato, M.; Schmidt, C.; Backes, C.; Hauke, F.; Hirsch, A. *Nat. Chem.* **2009**, *1*, 243.

(27) Tanaka, Y.; Hirana, Y.; Niidome, Y.; Kato, K.; Saito, S.; Nakashima, N. *Angew. Chem., Int. Ed.* **2009**, *48*, 1.

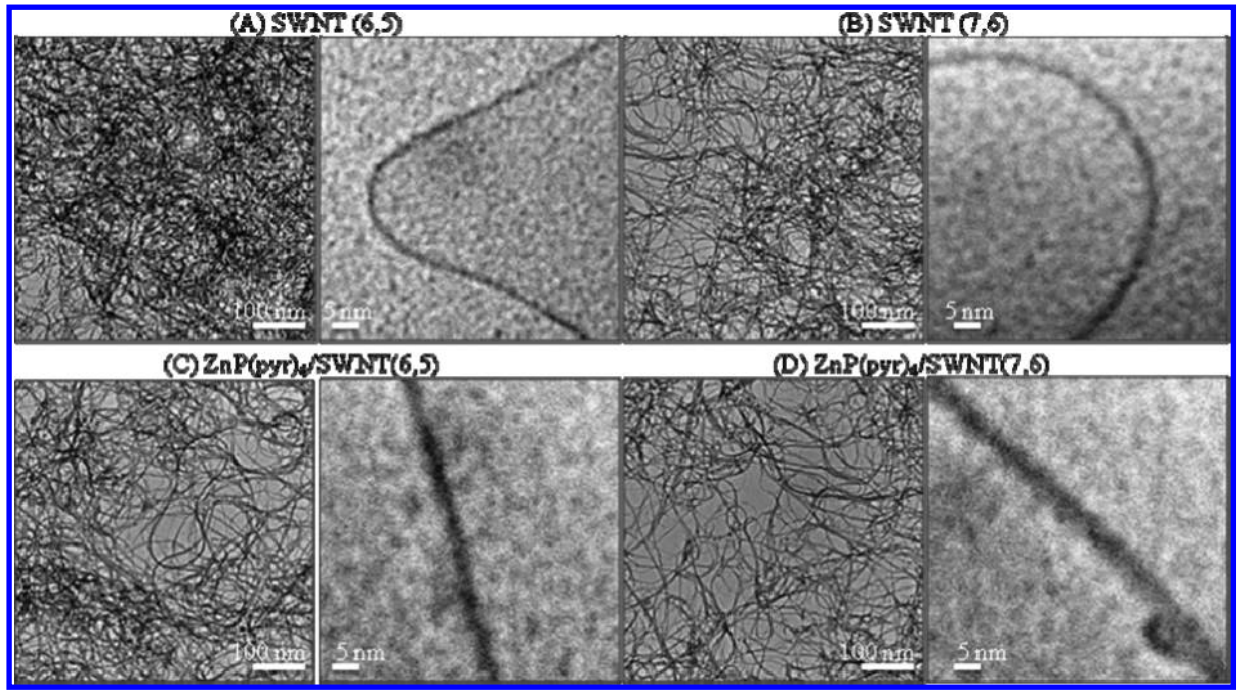

Figure 2. TEM images of (A) (6,5)-SWNT, (B) (7,6)-SWNT, (C) $ZnP(pyr)_4$/(6,5)-SWNT, and (D) $ZnP(pyr)_4$/(7,6)-SWNT at two magnification scales; white bar (left) 100 nm and (right) 5 nm.

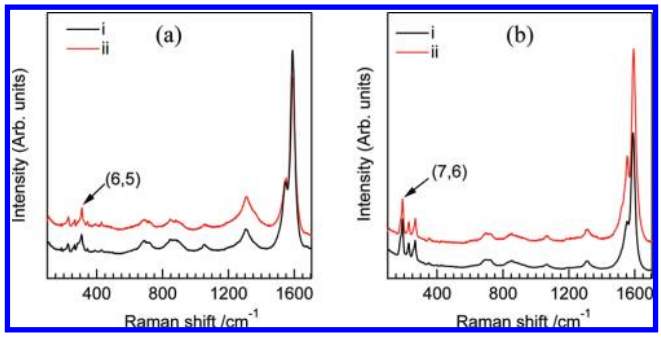

Figure 3. Raman spectra of (a) (i) $ZnP(pyr)_4$/(6,5)-SWNT and (ii) SWNT(6,5) and (b) (i) $ZnP(pyr)_4$/(7,6)-SWNT and (ii) SWNT(7,6) at the laser excitation wavelength of 632.8 nm.

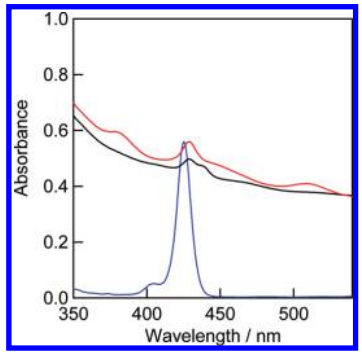

Figure 4. Steady-state absorption spectra in the Soret region of $ZnP(pyr)_4$/(6,5)-SWNT (black line), $ZnP(pyr)_4$/(7,6)-SWNT (red line), and $ZnP(pyr)_4$ (blue line) in DMF.

Steady-State Fluorescence Measurements. The formation of the $ZnP(pyr)_4$/(6,5)-SWNT and $ZnP(pyr)_4$/(7,6)-SWNT hybrids was also confirmed by fluorescence measurements, which also gave information about the excited state events in the hybrids. Figure 5 shows the steady-state fluorescence spectra (normalized to the intensity of the 614 nm band) of $ZnP(pyr)_4$, observed by

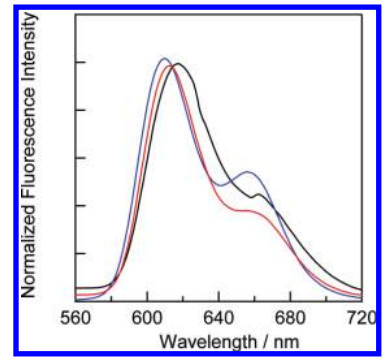

Figure 5. Steady-state fluorescence spectra of $ZnP(pyr)_4$/(6,5)-SWNT (black line), $ZnP(pyr)_4$/(7,6)-SWNT (red line), and $ZnP(Pyr)_4$ (blue line) in DMF; $\lambda_{ex} = 428$ nm; normalized at 614 nm.

the predominant excitation of the ZnP moiety (blue line), exhibiting a main peak around 614−620 nm with an additional 660 nm peak in DMF. Broadening with a slight peak shift was observed for (6,5)-SWNT and (7,6)-SWNT, supporting weak interaction between ZnP units and the SWNT surface. In the hybrids with SWNT, the ZnP fluorescence intensity was found to be quenched over 80% of its original intensity, suggesting the occurrence of excited-state events such as electron transfer and energy transfer.[14,19]

In order to obtain kinetics data for the singlet excited state of the ZnP moiety (^{1}ZnP*), picosecond time-resolved fluorescence measurements were performed with the streak-scope method. The time profiles collected in the ZnP fluorescence are shown in Figure 6. The ZnP fluorescence followed a monoexponential decay with a lifetime of 2100 ps. Addition of (6,5)-SWNT and (7,6)-SWNT to form the hybrids accelerated the ZnP fluorescence decay, which could be curve-fitted with a biexponential decay function. The ZnP fluorescence lifetimes evaluated under these conditions were found to be 260 (78%) and 2100 ps (22%) for $ZnP(pyr)_4$/(6,5)-SWNT and 180 (80%) and 2100 ps (20%) for $ZnP(pyr)_4$/(7,6)-SWNT, in which the

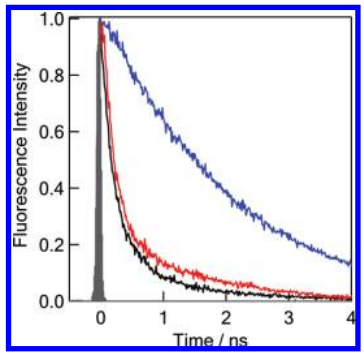

Figure 6. Fluorescence decays at monitoring region of 600−660 nm for ZnP(pyr)$_4$/(6,5)-SWNT (black line), ZnP(pyr)$_4$/(7,6)-SWNT (red line), and ZnP(Pyr)$_4$ (blue line) in DMF; $\lambda_{ex} = 408$ nm.

longer lifetime may be attributed to non-interacting ZnP(pyr)$_4$ with SWNTs. The fast-decaying component provides additional evidence for the formation the hybrids with SWNTs. By assuming that the fast-decaying component is due to electron transfer, the rate of charge separation, k_{CS}, and quantum yield, Φ_{CS}, were evaluated according to eqs 1 and 2.

$$k_{CS} = (1/\tau_f)_{nanohybrid} - (1/\tau_f)_{ref} \quad (1)$$

$$\Phi_{CS} = [(1/\tau_f)_{nanohybrid} - (1/\tau_f)_{ref}]/(1/\tau_f)_{nanohybrid} \quad (2)$$

where $(1/\tau_f)_{nanohybrid}$ and $(1/\tau_f)_{ref}$ are the lifetimes of the ^{1}ZnP* moiety in the presence and in the absence of SWNTs, respectively. The evaluated k_{CS} and Φ_{CS} in DMF were found to be 3.4×10^9 s^{-1} and 0.88 (0.69 including interacting fraction), respectively, for ZnP(pyr)$_4$/(6,5)-SWNT, which are slightly smaller than those for ZnP(pyr)$_4$/(7,6)-SWNT, that is, $k_{CS} = 5.1 \times 10^9$ s^{-1} and $\Phi_{CS} = 0.91$ (0.73 including interacting fraction) in DMF. These findings indicate that (7,6)-SWNT, with a narrower band gap, is more favorable for charge separation via ^{1}ZnP* compared with (6,5)-SWNT with wider band gap. Usually, semiconductors with narrower band gaps possess lower conduction bands having higher electron affinity, as supported by the reported E_{red} values.[27]

Nanosecond Transient Absorption Studies. Evidence for charge separation and the rate of charge recombination, k_{CR}, has been obtained from the transient absorption spectral studies using a 532-nm laser light, which predominantly excites the ZnP moiety.[28] Figure 7 shows the nanosecond transient absorption spectra of ZnP(pyr)$_4$/(7,6)-SWNT nanohybrids in Ar-saturated DMF (see Supporting Information, Figures S1 and S2, for (6,5)- and (7,6)-SWNT in the absence of ZnP). Importantly, a transient absorption peak corresponding to the formation of the ZnP radical cation (ZnP$^{\bullet+}$) around 600−700 nm[14a] was observed, although the ZnP$^{\bullet+}$ absorption may show slightly different features from the isolated ones because of appreciable perturbation from the near-by π-interacting SWNTs. In addition, the absorption bands in the near-IR region probably correspond to the trapped electron on the SWNTs (expressed as SWNT$^{\bullet-}$). Indeed, broad absorption bands observed around

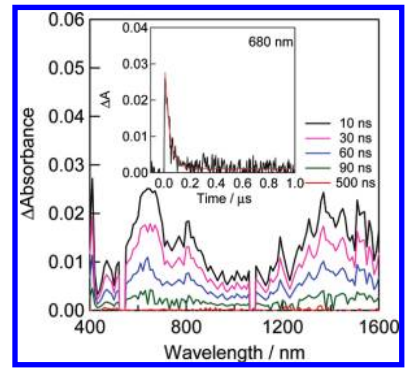

Figure 7. Nanosecond transient absorption spectra of ZnP(pyr)$_4$/(7,6)-SWNT observed upon 532 nm (ca. 3 mJ/pulse) laser irradiation in Ar-saturated DMF. Inset: Absorption−time profile.

1400 nm were frequently assigned to SWNT$^{\bullet-}$, although further studies are needed to confirm these assignments. The rise of ZnP$^{\bullet+}$ around 680 nm was estimated to be fast, within the nanosecond laser pulse (6 ns) (see the time profile in Figure 7 inset), which corresponds to the charge separation within ca. 2 ns as estimated from the ZnP fluorescence decay time profile (Figure 6), giving ZnP$^{\bullet+}$(pyr)$_4$/(7,6)-SWNT$^{\bullet-}$. The decay of ZnP$^{\bullet+}$ mostly finished within 200 ns; from the first-order fitting to the decay curve, the charge recombination rate constant of ZnP$^{\bullet+}$(pyr)$_4$/(7,6)-SWNT$^{\bullet-}$ was evaluated to be $k_{CR} = 2.7 \times 10^7$ s^{-1}. Using the k_{CR} value, the lifetime of the radical ion pair, τ_{RIP} ($= 1/k_{CR}$), was evaluated to be 37 ns, indicating that the radical ion pairs persist for some extent in the supramolecular nanohybrid in DMF.

For the ZnP(pyr)$_4$/(6,5)-SWNT, similar transient absorption spectra were observed (Supporting Information, Figure S3). From the time profile of ZnP$^{\bullet+}$, $k_{CR} = 2.1 \times 10^7$ s^{-1} and $\tau_{RIP} =$ ca. 48 ns in DMF were evaluated. These findings indicate that τ_{RIP} of ZnP$^{\bullet+}$(pyr)$_4$/(7,6)-SWNT$^{\bullet-}$ is slightly shorter than that of ZnP(pyr)$_4^{\bullet+}$/(6,5)-SWNT$^{\bullet-}$.

Electron-Pooling Measurements. In order to further confirm the occurrence of charge separation leading to the formation of ZnP$^{\bullet+}$(pyr)$_4$/SWNT$^{\bullet-}$, additional electron mediation experiments were performed by the addition of the second electron acceptor, hexyl viologen dication (HV^{2+}), and a sacrificial electron donor, 1-benzyl-1,4-dihydronicotinamide (BNAH), to the nanohybrid solution.[29] By steady-state absorption spectral measurements after repeated laser light irradiation (532 nm), which predominantly excites the ZnP moiety and SWNT but not the additives (HV^{2+} and BNAH), the accumulation of $HV^{\bullet+}$ was observed at 620 nm, as shown in Figure 8. The concentration of accumulated $HV^{\bullet+}$ species increased with increasing BNAH concentration, supporting the role of BNAH as a sacrificial hole-shifting reagent. In Figure 8, the overall maximal absorbance of $HV^{\bullet+}$ was observed in the presence of 0.5 mM HV^{2+} and 4.0 mM BNAH; thus, from the absorbance, the maximal concentration of $HV^{\bullet+}$ was evaluated to be 0.2 mM, which amounts to 40% conversion of added HV^{2+} for ZnP(pyr)$_4$/(6,5)-SWNT. For ZnP(pyr)$_4$/(7,6)-SWNT, the accumulation of $HV^{\bullet+}$ was similarly observed at 620 nm, giving the maximal concentration of 0.3 mM and 60% conversion. These observations indicate that ZnP(pyr)$_4$/(7,6)-SWNT is more efficient than ZnP(pyr)$_4$/(6,5)-SWNT for the accumulation of $HV^{\bullet+}$.

(28) The 532-nm laser light excites the shorter wavelength side of the Q-band of ZnP. Since the most of the broad absorption of SWNTs in the visible region is usually attributed to background, only small absorption of the SWNTs can be absorbed by the 532-nm laser light. It is difficult to evaluate the excited molecules quantitatively, because it depends on the abstraction of the background absorption and on the absorption coefficients, which are not possible to evaluate with reasonable accuracy for both the SWNT and absorbed ZnP in the hybrids.

(29) (a) Fukuzumi, S.; Suenobu, T.; Patz, M.; Hirasaka, T.; Itoh, S.; Fujitsuka, M.; Ito, O. *J. Am. Chem. Soc.* **1998**, *120*, 8060. (b) Pagona, G.; Sandanayaka, A. S. D.; Araki, Y.; Fan, J.; Tagmatarchis, N.; Yudasaka, M.; Iijima, S.; Ito, O. *J. Phys. Chem. B* **2006**, *110*, 20729.

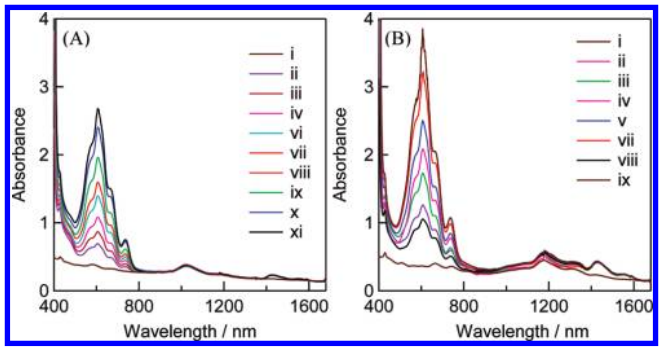

Figure 8. Steady-state absorption spectra of (A) ZnP(pyr)$_4$/(6,5)-SWNT and (B) ZnP(pyr)$_4$/(7,6)-SWNT in Ar-saturated DMF solution measured after five laser shots (6 ns pulse width and 3 mJ/pulse) at 532 nm in the presence of HV^{2+} (0.5 mM) and BNAH, (i) 0, (ii) 0.5, (iii) 1.0, (iv) 1.5, (v) 2.0, (vi) 2.5, (vii) 3.0, (viii) 3.5, and (ix) 4.0 mM.

Scheme 1[a]

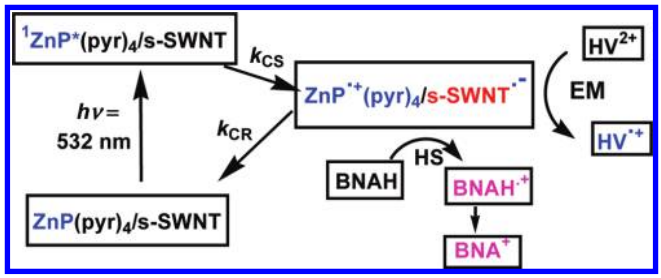

[a] Abbreviations: s-SWNT, semiconductor SWNT; CS, charge separation; CR, charge recombination; EM, electron migration; and HS, hole shift.

The mechanism for this electron-pooling process can be understood on the basis of the ZnP fluorescence quenching and transient absorption spectral measurements, suggesting generation of ZnP$^{\bullet+}$ and probable SWNT$^{\bullet-}$ in the nanohybrids. The electron trapped in SWNT transfers to HV^{2+}, generating $HV^{\bullet+}$ as the electron-pooling product. The hole of ZnP$^{\bullet+}$ irreversibly shifts to BNAH in the nanohybrids, giving BNAH$^{\bullet+}$, which is further converted to 1-benzylnicotinamide cation (BNA^+). The efficient photosensitized charge separation/electron migration/hole shift processes of the ZnP(pyr)$_4$/SWNT nanohybrids are illustrated in Scheme 1. The efficiency of the CS process vs the CR process can be evaluated from the ratio of k_{CS}/k_{CR}; the value of 190 for ZnP(pyr)$_4$/(7,6)-SWNT is higher than the value of 160 for ZnP(pyr)$_4$/(6,5)-SWNT, which can be defined as kinetic charge stabilization. This order is in agreement with the $HV^{\bullet+}$ accumulation conversion.

Photocurrent Measurements. A drop-cast method was applied to fabricate the films of ZnP(pyr)$_4$/SWNT adsorbing on the SnO_2 nanoparticles on the optical transparent electrodes (OTE/SnO_2 electrode). The absorption spectrum of OTE/SnO_2/ZnP(pyr)$_4$/SWNT is almost the same as those of ZnP(pyr)$_4$/SWNT shown in Figure 3 (see Supporting Information, Figure S4), except for the broadening of the absorption bands in the whole region, suggesting aggregation on the electrodes.

Photoelectrochemical measurements were performed in a two-compartment cell equipped with a potentiostat, using OTE/SnO_2/ZnP(pyr)$_4$/SWNT as the working electrode and Pt wire as the counter electrode.

The photocurrent action spectra of OTE/SnO_2/ZnP(pyr)$_4$/SWNT electrodes were measured by examining the wavelength dependence of the incident photon-to-current conversion efficiency (IPCE).[30] The IPCE values are calculated by normalizing the photocurrent densities for incident light energy and intensity in the usual manner. As shown in Figure 9, the IPCE of OTE/SnO_2/ZnP(pyr)$_4$/(7,6)-SWNT electrode reaches 1% as a maximal value at 420 nm, with the second maximum near 460 nm, which is about 3 times larger than that of OTE/SnO_2/ZnP(pyr)$_4$/(6,5)-SWNT electrode (0.35% in 400−450 nm region). This order is in agreement with those of the $HV^{\bullet+}$ accumulation conversion and k_{CS}/k_{CR}.

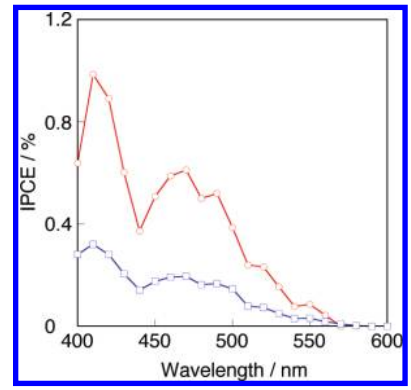

Figure 9. Photocurrent action spectra of IPCE: OTE/SnO_2/ZnP(pyr)$_4$/(6,5)-SWNT electrode (blue spectrum) and OTE/SnO_2/ZnP(pyr)$_4$/(7,6)-SWNT electrode (red spectrum). Electrolyte: 0.5 M LiI, 0.01 M I_2 in acetonitrile.

Summary

The first report on photoinduced electron transfer in self-assembled zinc porphyrin−SWNT hybrids having (7,6)- and (6,5)-enriched carbon nanotubes is documented. The zinc porphyrin, along with four pendant pyrene entities (ZnP(pyr)$_4$), stacked on the SWNT surface due to $\pi-\pi$ interactions, resulting in exfoliation of the semiconducting nanotubes, as revealed by TEM measurements. Raman spectral measurements revealed the electronic structure of the nanotubes to be intact upon hybrid formation. Free-energy calculations suggested the possibility of photoinduced electron transfer in both the (7,6)- and (6,5)-enriched ZnP(pyr)$_4$/SWNT nanohybrids, while steady-state and time-resolved fluorescence studies revealed efficient charge separation quenching via the singlet excited state of zinc porphyrin, as supported by the nanosecond transient absorption technique, which confirmed the porphyrin cation radical. The rates of charge separation, k_{CS}, was found to be slightly higher for (7,6)-nanotube-derived hybrids than for (6,5)-nanotube-derived hybrids, while an opposite trend was observed for k_{CR}. The nanohybrids also photocatalytically reduced hexyl viologen dication (HV^{2+}) and oxidized a sacrificial electron donor in an electron-pooling experiment, offering additional proof for the occurrence of photoinduced charge separation. Finally, solar cells constructed using the ZnP(pyr)$_4$/SWNT hybrids yielded an interesting result, showing that the efficiency of the solar energy conversion was higher for (7,6)-SWNT, with a narrower band gap, compared with (6,5)-SWNT, having a wider band gap, following the same trends observed with charge separation and electron pooling processes.

Experimental Section

Chemicals. The (6,5)- and (7,6)-enriched SWNTs were produced by CoMoCAT, SouthWest Nano Technologies, Inc. (Norman, OK),

(30) IPCE(%) = 100 × 1240 × $I_{SC}/(W_{in}\lambda)$, where I_{SC} is the short circuit photocurrent (A/cm^2), W_{in} is the incident light intensity (W/cm^2), and λ is the wavelength in nm.

marketed by Aldrich Chemicals (Milwaukee, WI). The bulk solvents utilized in the syntheses were from Fischer Chemicals, while all of the chemicals used in the synthesis of pyrene-appended porphyrin were from Aldrich Chemicals.

Synthesis of Pyrene Functionalized Zinc Porphyrin. (4-Formyl)phenyl 4-Pyrenylbutanoate (1). 1-Pyrenebutyric acid (590 mg, 2.05 mmol) and 4-hydroxybenzaldehyde (750 mg, 6.00 mmol) were dissolved in 150 mL of dry CH_2Cl_2, and then 1,3-dicyclohexylcarbodiimide (600 mg, 2.25 mmol) and 4-(dimethylamino)pyridine (32 mg, 0.524 mmol) were added. The reaction mixture was stirred for 18 h. The solvent was then evaporated under reduced pressure, and the crude compound was purified on a silica gel column using hexane/CH_2Cl_2 (94:6 v/v) as eluent. Yield: 170 mg (20%). ^{1}H NMR (400 MHz, $CDCl_3$) (in ppm): δ 9.99 (s, 1H, −CHO), 8.33−7.83 (m, 13H, pyrene *H* and phenyl *H*), 3.50 (t, 2H, $-CH_2-$), 2.75 (t, 2H, $-CH_2-$), 2.33 (m, 2H, $-CH_2-$). Mass (APCI mode in CH_2Cl_2): calcd, 392.45; found, 393.80.

H_2-5,10,15,20-Tetra(phenyl-4-pyrenylbutanoyl)porphyrin (2). The title compound was synthesized according to Lee and Lindsey.[31] Pyrrole (100 μL, 1.42 mmol) and **1** (558 mg, 1.42 mmol) were dissolved in 200 mL of dry $CHCl_3$, and the resultant mixture was stirred under argon for 1.5 h. $BF_3 \cdot O(Et)_2$ (60 μL, 0.473 mmol) was then added. Porphyrin formation leveled off after 1 h. *p*-Chloronil (265 mg, 1.07 mmol) was then added to the reddish-black reaction mixture, and the resultant mixture was stirred at room temperature for 1 h. Triethylamine (66 μL, 0.473 mmol) was added, and the reaction mixture was stirred for 8 h and then concentrated. Column chromatography on silica gel using hexane/$CHCl_3$ (60:40 v/v) as eluent gave compound **2**. Yield: 52 mg (5%). ^{1}H NMR (400 MHz, $CDCl_3$) (in ppm): δ 8.89 (s, 8H, β pyrrole), 8.49−7.50 (m, 52H, pyrene *H* and phenyl *H*), 3.61 (t, 8H, $-CH_2-$), 2.90 (t, 8H, $-CH_2-$), 2.41 (m, 8H, $-CH_2-$), −2.81 (s, 2H, −NH−). Mass (APCI mode in CH_2Cl_2): calcd, 1760.03; found, 1761.0.

5,10,15,20-Tetra(phenyl-4-pyrenylbutanoyl)porphyrinatozinc(II) (3). The free-base porphyrin **2** (25 mg) was dissolved in $CHCl_3$ (10 mL), a saturated solution of zinc acetate in methanol was added, and the resulting mixture was refluxed for 2 h.[32] The course of the reaction was followed by monitoring the disappearance of the 512-nm absorption band of **2**. At the end, the reaction was washed with water and dried over anhydrous Na_2SO_4. Chromatography on a silica gel column using $CHCl_3$ as eluent gave compound **3**. Yield: 90%. ^{1}H NMR (400 MHz, $CDCl_3$) (in ppm): δ 9.00 (s, 8H, β pyrrole), 8.41−7.21 (m, 52H, pyrene *H* and phenyl *H*), 3.60 (t, 8H, $-CH_2-$), 2.88 (t, 8H, $-CH_2-$), 2.46 (m, 8H, $-CH_2-$). Mass (APCI mode in CH_2Cl_2): calcd, 1823.43; found, 1824.8.

Preparation of ZnP(pyr)$_4$/(6,5)-SWNT and ZnP(pyr)$_4$/(7,6)-SWNT Nanohybrids. A 1.0 mg sample of SWNT [(6,5) or (7,6) chirality] was added to 2.10 mg of $ZnP(pyr)_4$ dissolved in 15 mL of dry DMF, and the reaction mixture was stirred for 48 h at room temperature. The resulting mixture was sonicated (Fisher Scientific, 60 Hz, 40 W) for 6 h at 20 °C, followed by centrifugation (Fisher Scientific, 50/60 CY) for 2 h. The excess of porphyrin was removed by separating the centrifugate from the black precipitate. Further purification was carried out by dissolving the black mixture in 5 mL of fresh DMF and sonicating for 30 min at 20 °C, followed by centrifugation for 1 h and removal of unadsorbed porphyrin by separation from the black centrifugate. This process was repeated (at least twice) until the solution in the centrifuge tube turned colorless. At the end, 10 mL of fresh solvent was added to the resulting deposit and was sonicated for 15 min at 20 °C. This homogeneous black dispersion was stable for several days and used as mentioned in subsequent studies.

Instrumentation. The UV−visible−NIR spectral measurements were carried out with a Perkin-Elmer (Lamda 750) or Jasco V-670 spectrophotometer. The steady-state fluorescence emission was monitored by using a Perkin-Elmer (LS-55) or a Horiba Jobin Yvon Nanolog UV−vis−NIR spectrofluorometer equipped with PMT (for UV−vis) and InGaAs (for NIR) detectors. The ^{1}H NMR studies were carried out on a Varian 400 MHz spectrometer. Tetramethylsilane (TMS) was used as an internal standard. All the solutions were purged prior to spectral measurements using nitrogen gas.

Transmission electron micrograph (TEM) measurements were recorded by applying a drop of the sample to a copper grid. Images were recorded on a Hitachi H-7650 TEM at an accelerating voltage of 120 kV. A TEM equipped with EDX (H-2300, Hitachi) was operated at 120 kV, and the elemental map was obtained by using a scanning spot size of 0.5 nm and a scanning rate of 0.5 nm/ms.

Raman spectroscopy measurements were performed using a Tokyo Instruments Nanofinder 30) with three different laser excitations, namely, $\lambda = 441.6$ (HeCd), 532.0 (Nd:YAG), and 632.8 nm (HeNe), and the laser spot size was about 2 mm in diameter.

The time-resolved fluorescence spectra were measured by a single-photon-counting method using a streakscope (Hamamatsu Photonics, C5680) as a detector and a laser light (Hamamatsu Photonics M10306, laser diode head, 408 nm) as an excitation source. Lifetimes were evaluated with software attached to the equipment.

Nanosecond transient absorption measurements were carried out using third harmonic generation (532 nm) of a Nd:YAG laser (Spectra-Physics, Quanta-Ray GCR-130, 5 ns fwhm) as an excitation source. For transient absorption spectra in the near-IR region (600−1200 nm) and the time profiles, monitoring light from a pulsed Xe lamp was detected with a Ge-APD (Hamamatsu Photonics, B2834). For the measurements in the visible region (400−1000 nm), a Si-PIN photodiode (Hamamatsu Photonics, S1722-02) was used as a detector.

Photoelectrochemical measurements were carried out in a standard two-compartment cell consisting of a working electrode and a Pt wire gauze counter electrode in the electrolyte. The electrolyte was 0.5 M LiI and 0.01 M I_2 in acetonitrile. In the case of IPCE measurement, a monochromator (SM-25, Bunkoh-Keiki Co., Ltd.) was introduced into the path of the excitation beam (300-W xenon lamp, Bunkoh-Keiki Co., Ltd.) for the selected wavelength. The lamp intensity at each wavelength was determined by using a Si photodiode (Hamamatsu Photonics S1337-1010BQ) and corrected.

Acknowledgment. This work was financially supported by the National Science Foundation (Grant Nos. 0804015 and EPS-0903806) and matching support from the State of Kansas through Kansas Technology Enterprise Corp. This study was also supported by Grant-in-Aid for Scientific Research (No. 21710104 to T.H.) from Ministry of Education, Culture, Sports, Science and Technology, Japan, and to A.S.D.S. from the Japan Society for the Promotion of Science (JSPS). We thank Prof. H. Murata of JAIST for his support.

Supporting Information Available: Transient absorption spectra of (6,5)-SWNT, (7,6)-SWNT, and ZnP(pyr)$_4$/(6,5)-SWNT, absorption spectra of OTE/SnO_2/SWNT electrodes, and complete ref 7e. This material is available free of charge via the Internet at http://pubs.acs.org.

JA101776P

(31) Lee, C. H.; Lindsey, J. S. *Tetrahedron* **1994**, *50*, 11427.
(32) Smith, K. M. *Porphyrins and Metalloporphyrins*; Elsevier: Amsterdam, 1972.